Vortex shedding and aerodynamic performance of an airfoil with multi-scale trailing edge modifications

J. Nedić * and J.C. Vassilicos †

Turbulence, Mixing and Flow Control Group, Department of Aeronautics

Imperial College London, Prince Consort Road, London SW7 2AZ, UK

An experimental investigation was conducted into the nature of the vortex shedding generated by truncated and non-flat serrated trailing edges of a NACA 0012 wing section, as well as the aerodynamic performance of such trailing edges. In-line with previous findings, the truncated trailing edge generates a significant amount of vortex shedding, whilst increasing both the maximum lift and drag coefficients, resulting in an overall reduction in the maximum lift-to-drag ratio compared to a plain NACA0012 wing section. By decreasing the chevron angle (φ) of the non-flat trailing edge serrations (i.e. by making them sharper), the energy of the vortex shedding significantly decreases and the lift-to-drag ratios increase compared to a plain NACA0012 wing section. Fractal / multi-scale patterns made of scaled-down repetitions of these serrations were also investigated with a view to further improve performance. It was found that the energy of the vortex shedding increases with increasing fractal iteration if the chevron is broad ($\varphi \approx 65°$), but decreases for sharper chevrons ($\varphi = 45°$). It is believed that if φ is too big, the multi-scale trailing edges are too far away from each other to interact and break down the vortex shedding mechanism. Fractal/multi-scale trailing edges are also able to improve aerodynamic performance compared to the NACA 0012 wing section.

Nomenclature

C_D Drag coefficient

*Research Associate, Department of Aeronautics, Imperial College London, AIAA Member. Current Position: Postdoctoral Fellow, Department of Mechanical Engineering, University of Ottawa

†Professor, Department of Aeronautics, Imperial College London

C_L Lift coefficient

c Mean chord length of wing section, m

c^* Maximum chord length of wing section, m

D_f Fractal dimension

E_{11} Energy spectrum of streamwise velocity normalised with freestream velocity, Hz^{-1}

f Frequency, Hz

L/D Lift-to-drag ratio

P Peak location

T Trough location

U_∞ Freestream velocity (ms^{-1})

St Strouhal number

x streamwise direction measured from the leading edge of the wing, m

y wing normal direction measured from the leading edge of the wing, m

z spanwise direction measured from the leading edge of the wing, m

α Angle of attack, deg

γ Coherence of the streamwise velocities in the wake

Δ Difference between two values

ΔSt Non-dimensional frequency bandwidth

ε_{max} Maximum thickness of exposed bluntness of wing section, mm

λ Wavelength of chevron, mm

φ Chevron angle, deg

ξ Energy of vortex shedding in space, a.u.

$\mathcal{P}/S$ Ratio between total length of trailing edge to span of wing section

$2h$ Peak-to-trough distance, mm

Subscript

i Fractal iteration

n Wing identification number

vs Quantity at vortex shedding frequency

I. Introduction

RECENTLY, there has been a growing trend of modifying wing sections in order to obtain improved aerodynamic and acoustic performance. Early modifications focussed on truncating the trailing edge of an airfoil section which was achieved by simply removing a given amount from an already existing wing section.[1] These modifications were found to increase the maximum lift coefficient compared to an unmodified wing section at a constant chord Reynolds number, however the now exposed bluntness also increased the drag coefficient as well as creating strong von-Karman type shedding.[2] Tanner,[3] for example, addressed this issue by employing broken, curved and serrated trailing edges onto a blunt trailing edge section and found a drag reduction of up to 65% could be achieved compared to the blunt trailing edge. Similar reductions of up to ~ 40% were found by Rodriguez[4] on a blunt two-dimensional body and ~ 30% on a truncated NACA0012 wing section by Krentel & Nitsche,[5] both of which used similar trailing edge modifications to Tanner. This reduction in drag coefficient was found to be related to the weakening of the intensity of the spanwise coherent structures created by the von-Karman type shedding, as well as the two-dimensional nature of these structures. Tombazis & Bearman[6] observed similar results using a blunt sinusoidal trailing edge on a blunt two-dimensional body. Other novel trailing edge modifications include the study by Werle et al.,[7] who used a non-planar sinusoidal trailing edge and found an increase in the maximum lift coefficient and lift curve slope; these changes were believed to be due to the creation of streamwise vortices that alleviated the pressure gradient on the surface of the wing, thus delaying stall.

Inspired by turbucules found on humpback whales which have been shown to increase the lift coefficient in the post-stall region, thus increasing the manoeuvrability of the whale,[8–10] there has also been growing interest in using leading edge modifications. Hansen et al,[11] for example, used a planar sinusoidal leading edge on a two-dimensional (as opposed to the finite wing sections that were used by[8–10]) NACA 65-021 and NACA0021 wing section, where they found a similar increase in lift coefficient in the post-stall region, but a reduction in lift in the pre-stall region for the NACA0021 wing. However, by optimising the dimensions of the leading edge geometry, they were able to improve the performance in both the pre-stall and post-stall regions. Rostamzadeh et al[12] used non-planar sinusoidal leading edges on a NACA0021 wing section and found similar pre- and post-stall behaviours as for the planar sinusoidal leading edges. The increase in lift coefficient in the post-stall region for both of these trailing edges was attributed to the creation of counter-rotating streamwise vortices, similar to the non-planar

sinusoidal trailing edges of Werle et al.,[7] which were clearly visible in the near wake of the wings.

From an acoustic point of view, considerable attention has been paid to trailing edge noise. Following the work by Howe,[13] serrated trailing edges have been the tool of choice for many studies.[14–16] These serrated trailing edges were, both numerically and experimentally, attached onto the trailing edge of the wing section which would have unfavourable structural properties as they were likely to vibrate during operation. For this reason Chong et al[17] investigated the noise generated by non-flat trailing edge serrations, where the serrations were cut directly into the wing itself, thus preserving the overall wing profile and adding structural integrity to the serrations. They found a larger reduction in the sound pressure level (SPL) at higher frequencies compared to the case when a serrated flat plate was attached onto the wing (in both cases with a turbulent boundary layer present on both surfaces of the wing). However, a noticeable increase in low frequency noise was observed which was believed to be due to the vortex shedding being created by the now exposed bluff trailing edge. The impact of this low frequency noise, which dominated the overall noise of the airfoil, was reduced by changing the angles of the serrations used. Other methods, such as porous wings[18] for example, have also been attempted which showed a reduction of 10dB in the sound pressure level; however, there was an overall reduction in lift and increase in drag of the wing itself.

Both the aerodynamic and acoustic studies have shown that by weakening the vortex shedding mechanism, reductions in drag and low frequency noise can be obtained. Recently it has been shown that by adding successive iterations of a given pattern along the perimeter of a bluff flat plate in a fractal/multi-scale manner, the intensity of the large-scale structures decreased.[19,20] Similarly, by increasing the fractal dimension the intensity decreased even further. However, one surprising result was that the drag coefficient increased for these 'fractal plates' which were placed with their area facing the flow.[19,21] In this study, we aim to investigate the feasibility of using similar fractal/multi-scale patterns but applied to the trailing edge of a wing section. The aim is to break down the intensity of the large-scale structures generated by a wing with a bluff trailing edge without damaging, in fact by even ideally improving, aerodynamic performance.

II. Experimental set-up

A. Test model and trailing-edge design

In order to investigate the various trailing edge options, all trailing edges are inserted into a base wing model, as shown in figure 1. This model has a NACA0012 profile, a span of $S = 455mm$ and a chord length of $c^* = 150mm$. From $x/c^* = 0$ (leading edge) to a distance of $x = 0.75c^*$, the section is unchanged; from this point on, a section of length $x = 0.25c^*(37.5mm)$ and width 420mm (S') is cut away leaving small solid sections at the edges of the wing. This main wing section is coloured in blue in figure 1(a). To reduce manufacturing time and costs, a trailing edge mount (grey element in figure 1(a)) is attached onto the end of the main wing section. The trailing edges, shown as red in figure 1(a), are then attached onto this mount. When the trailing edges are inserted onto the wing, the chord length at any point along the span never exceeds the reference chord c^*. With the trailing edges inserted they form a continuous profile and give the appearance that the trailing edges are cut into a NACA0012 wing section. All parts were manufactured using a Connex350 3D printer, with RGD5160-DM (FullCure®515 + FullCure®535) as the material. The build resolution of the printer is $30\mu m$ in the plane of the build tray, whilst the depth resolution is $16\mu m$ (i.e. the material thickness is $16\mu m$ thick for each stage of the build); the accuracy of the final build is stated to be between 20-85μm for builds less than 50mm in height, which all of our parts were. The wing was also sanded down and painted to create a smooth surface finish and a roughness element (very course sandpaper) is placed at $x = 0.2c^*$ from the leading edge on both sides of the airfoil to ensure a turbulent boundary layer is created. The design of the test model is very similar to the one used by Chong et al.[17]

A total of nine trailing edges were investigated the details of which can be found in table 1; seven of these trailing edges are shown in figure 2. Wing 1 is a plain NACA 0012 trailing edge i.e. no modifications were made. Wing 2 is a truncated wing section with a constant bluntness of $\varepsilon = 5.56mm$ along the span, this bluntness corresponding to the reference chord length c^* being truncated by 20mm from the trailing edge of the NACA0012 wing. Figure 1 shows the definitions of various chevron trailing edge parameters, such as l_1, λ, φ and β, which are used to define Wings 3, 6 and 9. Following Chong et al,[17] we set the peak-to-trough distance as $2h = 20mm$ (see figure 1(c)), the primary reason being that it allows for easy comparison with their data.

The fractal/multi-scale trailing edges (Wings 4, 5, 7 and 8 in figure 2) are created by applying a scaled

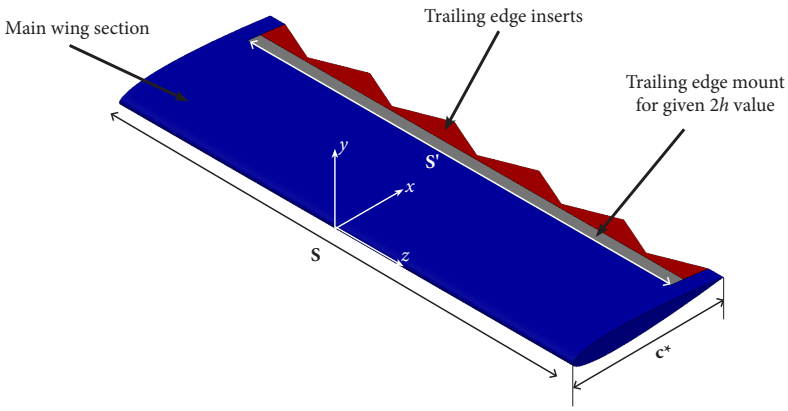

(a) Main wing and trailing edge geometry definitions - Wing 3 shown here

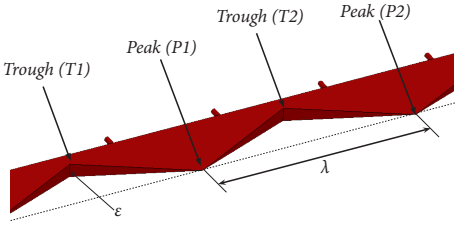

(b) *Peak* and *Trough* definition

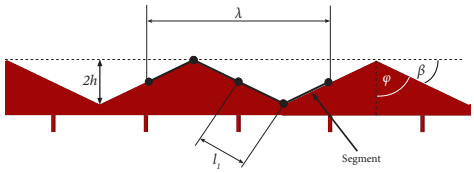

(c) Chevron definitions and base chevron shape shown between the five nodes

Figure 1. Drawing of main wing and trailing edges, showing the definitions of various parameters.

down version of the base chevron pattern (shown in figure 1(c)) onto each segment and then repeating this process on each newly created segment of length l_i (at iteration $i-1$). The number of segments which create the trailing edge shape increases with the iteration number as 4^i, where the number 4 refers to the number of segments required to create the base shape i.e. 4 segments of equal length are required to create the chevron pattern used here. Newly created segments at iteration i have a length l_i, with the scaling ratio between successive iterations (r) defined in equation 2. The main advantage of using fractal patterns is that it allows the user to introduce a variety of length-scales whilst increasing the total length of the trailing edge $\mathcal{P}$, without increasing the wing surface area (except for the fact that c^* is the maximum chord, a constraint which actually imposes a small decrease in area from iteration $i=2$ to iteration $i=3$). The equations for r, $\mathcal{P}$ and the fractal dimension D_f of the fractal trailing edges, in terms of the angle $\beta = \frac{\pi}{2} - \varphi$, λ, l_i and S (the span of the wing) are:

$$D_f = \frac{\log 4}{\log r} \tag{1}$$

$$r = 4\cos\beta = \left(\frac{\lambda}{l_i}\right)^{1/i} \tag{2}$$

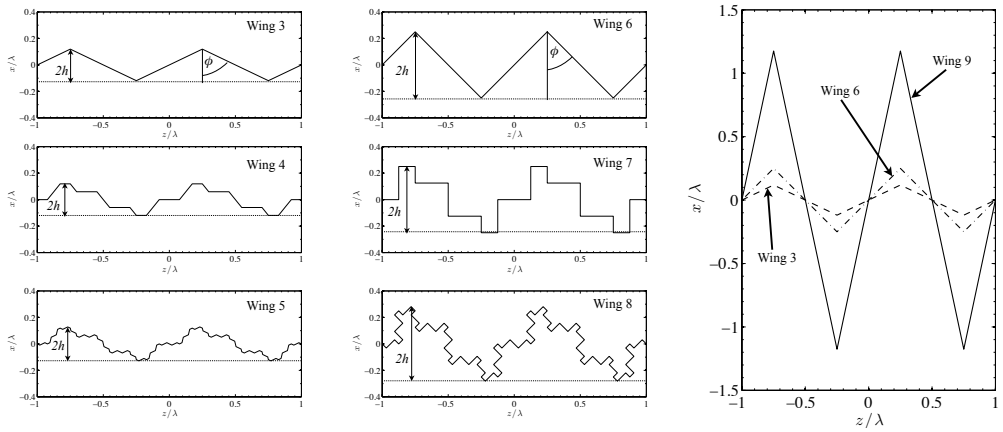

Figure 2. Trailing edges under investigation. Left column is for successive iterations of the $D_f = 1.08$ family of trailing edges; centre column for successive iterations of the $D_f = 1.33$ family of trailing edges and right for chevron based patterns. Each successive iteration is created by applying the base chevron pattern to segments created in the previous iteration.

$$\lambda \tan \beta = 4h \tag{3}$$

$$\mathcal{P} = \frac{4^i l_i S}{\lambda} \tag{4}$$

Note that to fully define these trailing edges, one needs to choose values for λ, β and the number of iterations. A larger fractal dimension signifies a 'rougher' trailing edge in the case of multiple iterations.

Although Chong et al[17] only consider chevron patterns whose angles are less than $\varphi = 45°$, as theoretically these angles would give the largest reduction in sound pressure level (SPL),[13] our chevron based trailing edge modifications are limited to angles greater than $\varphi \approx 34°$, since any fractal/multi-scale based modifications below this angle would not be physically possible because of the constraint $D_f < 2$.

Wing 3 (table 1) has a large wavelength λ (distance between successive peaks) compared to the $2h$ value, which results in a gentle perturbation similar to the sinusoidal edge modifications studied by Tombazis & Bearman.[6] As one would expect, this 'smooth' trailing edge has a low fractal dimension of $D_f = 1.08$. Successive iterations of the trailing edge are then created by applying the same chevron pattern to each segment of the previous iteration. The maximum number of iterations was set to three since above this value the length of the smallest segments exceed the tolerance of the 3D printer which was used to manufacture them. Wings 6 - 8 have the same fractal/multi-scale design as the $D_f = 4/3$ fractal plates in Nedic et al.[19] Wing 9 is the same as wing $S2$ in Chong et al.[17] Owing to the way

Wing no. (n)	D_f	i	$\lambda(mm)$	$l_i(mm)$	$\varepsilon_{max}(mm)$	$\varphi(^\circ)$	$2h(mm)$	$\mathcal{P}/S$	Symbol
1	1	1	420	0.00	0.00	0.00	0.00	1.00	•
2	1	1	420	0.00	5.56	0.00	20.00	1.00	□
3	1.08	1	84	23.26	5.56	64.54	20.00	1.11	▲
4	1.08	2	84	6.44	5.56	64.54	20.00	1.23	▶
5	1.08	3	84	1.78	5.75	64.54	21.54	1.36	▼
6	1.33	1	40	14.14	5.56	45.00	20.00	1.41	△
7	1.33	2	40	5.00	5.56	45.00	20.00	2.00	▷
8	1.33	3	40	1.77	5.86	45.00	22.50	2.82	▽
9	-	1	8.5	10.22	5.56	12.00	20.00	4.81	⋆

Table 1. Trailing edge classification showing iteration number i, wavelength of pattern λ, maximum exposed bluntness ε_{max}, chevron angle φ, peak to trough distance $2h$, ratio between length of trailing edge to span of wing $\mathcal{P}/S$ and the symbols that will be used in subsequent figures for each of the trailing edges.

that the multi-scale trailing edges are created, the last iterations ($i = 3$) of both fractal dimensions have $2h > 20mm$, as shown in table 1. Since we impose that the local chord length does not exceed c^*, it means that for these trailing edges we have to go further into the wing, resulting in a larger maximum exposed bluntness ε_{max}.

B. Wind tunnel and measurements

A blow down wind tunnel, with a test section of $0.4572m \times 0.4572m$ (18 inch x 18 inch) in size and a working length of 3.5m was used for all the measurements. The tunnel has a background turbulence level of 0.1%. The wing was mounted 1.5m downstream of the 8-1 contraction, with the inlet velocity set so that the Reynolds number based on the mean chord of the airfoil, as defined in equation 5, was $Re_c = U_\infty c/\nu = 150,000$.

$$Sc = Sc^* - S'h \tag{5}$$

For the force measurements, the wing was mounted vertically onto an ATI Gamma65 F/T sensor. The sensor has a range of 65N and resolution of 0.0125N in the normal and axial directions, the axis of which are defined along the chord line of the airfoil, and an uncertainty estimate of ±1%. For our measurements, we estimate a maximum measurement uncertainty of 0.01 in the lift and drag coefficient, and 0.5 for the lift-to-drag ratio. Both the wing and the sensor were mounted onto a stepper motor which had an optical encoder attached, hence allowing for the sensor and wing to be rotated for a range of angles with an accuracy of 0.088°. Measurements were taken between $0^\circ \leq \alpha \leq 18^\circ$, where α is the angle of attack. At the highest angle of attack, the blockage ratio was 10%. As Wing 1 is the baseline

comparison for our aerodynamic force measurements, no blockage corrections were applied to the data. Data was sampled for 30s at each angle of attack, and each experiment was repeated a total of 10 times in order to get an estimate of the experimental error in the measurements. Owing to the orientation of the wing relative to the sensor and the fact that both sensor and wing rotated together, the sensor measures the wing normal (N_f) and axial forces (A_f), which are converted into lift (L) and drag (D) force using equations 6 and 7. Hence the resolution of lift and drag force measurements are functions of the angle of attack and is found to range between 0.0125N - 0.008N for the lift force and 0.0125N - 0.0158N for the drag force as the angle of attack is increased from $\alpha = 0°$ to $\alpha = 18°$ respectively. This corresponds to a resolution in the lift and drag coefficient of ~ 0.001. The zero angle of attack was found at the start of each of the ten runs for each trailing edge by acquiring force measurements for angles between $-5° \leq \alpha \leq 5°$ which gave a linear variation in the lift coefficient; the wing was then rotated to the angle that gave zero lift and the process repeated a further two times.

$$L = N_f \cos\alpha - A_f \sin\alpha \tag{6}$$

$$D = N_f \sin\alpha + A_f \cos\alpha \tag{7}$$

Flow measurements were also taken in the wake of the wing model, for which the wing was mounted horizontally in the wind tunnel at an angle of attack of $\alpha = 5°$, giving a blockage ratio of 2.85%. To investigate the vortex shedding, three single hot-wire probes ($5\mu m$ in diameter with a sensing length of 1.25mm, DANTEC 55P01), measuring the streamwise velocity component, were placed in the wake and driven by a DANTEC Streamline CTA. Data was sampled simultaneously for $15s$ at a sampling frequency of 40kHz, with the data then being low-pass filtered at 10kHz. The post processing of this data was concerned with the statistics of the fluctuating streamwise velocity.

III. Vortex shedding behaviour

A. Identification of vortex shedding structures

To investigate the vortex shedding in the wake, three hot-wire probes were positioned to coincide with successive *trough-peak-trough* ($T_1 - P_1 - T_2$) z locations (the distance between T_1 and T_2, and similarly between P_1 and P_2, is λ - see figure 1(b)), at a downstream distance of $x = 1.1c^*$ from the leading edge

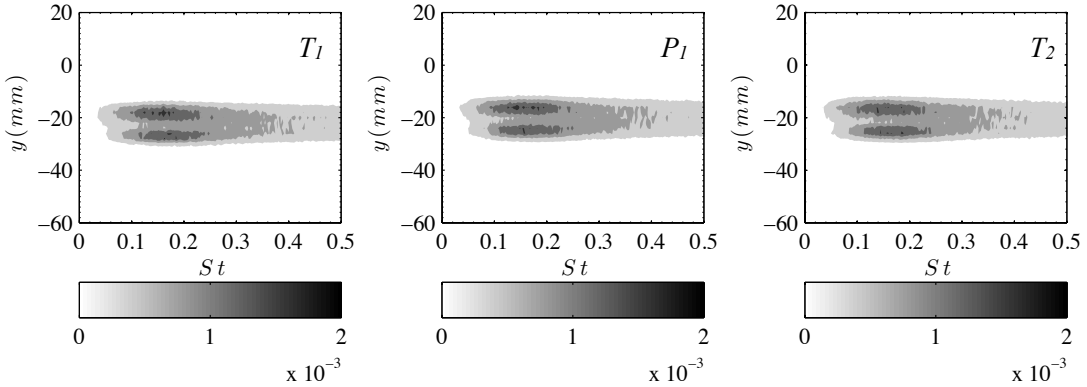

(a) Wing 1

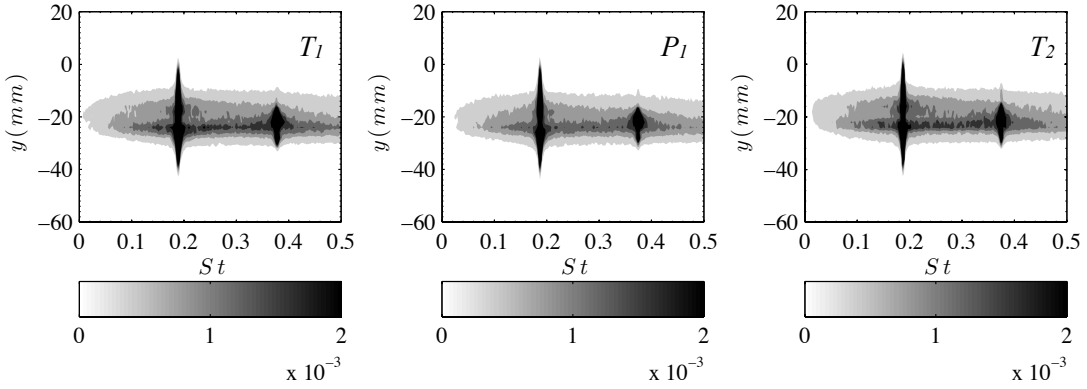

(b) Wing 2

Figure 3. Contour plot of pre-multiplied energy spectra (i.e. fE_{11}) at $x = 1.1c^*$ for successive *trough-peak-trough* locations (left to right) for Wings 1 and 2

and traversed in y. Note that for Wing 2, the positions of the probes correspond to the $T_1 - P_1 - T_2$ locations for Wings 3-6, and for Wing 9 they correspond to the $T_1 - P_1 - T_2$ locations for Wings 6-8. The reason for this is that the spacing between two successive troughs, i.e. the wavelength λ, is 8.5mm for Wing 9 and due to the way in which the probes were mounted, it was not possible to achieve this spacing safely without any fear of damage to the hot-wires or interference in the signal from neighbouring wires. The central of the three probes is located at a *peak* location for Wing 9, however, the probes either side of it are at $z \approx \pm 2.35\lambda$, which would place them close to a trough, but not the closest ones.

In figure 3, we show a contour plot of the pre-multiplied energy spectra of the stream-wise fluctuating velocity component (i.e. fE_{11}) for Wing 1 and Wing 2 at all wing-normal positions (y axis in figure 1(a)), taken at a downstream distance of $x = 1.1c*$, and for all three hot-wire probe locations. The frequency f on the x-axis in figure 3 has been normalised to create a Strouhal number based on the bluntness of the trailing edge i.e. $St = f\varepsilon_{max}/U_\infty$ (ε_{max} is defined as the maximum bluntness thickness of the trailing edge, but for Wing 2 this bluntness is uniform along the span and therefore trivially equal

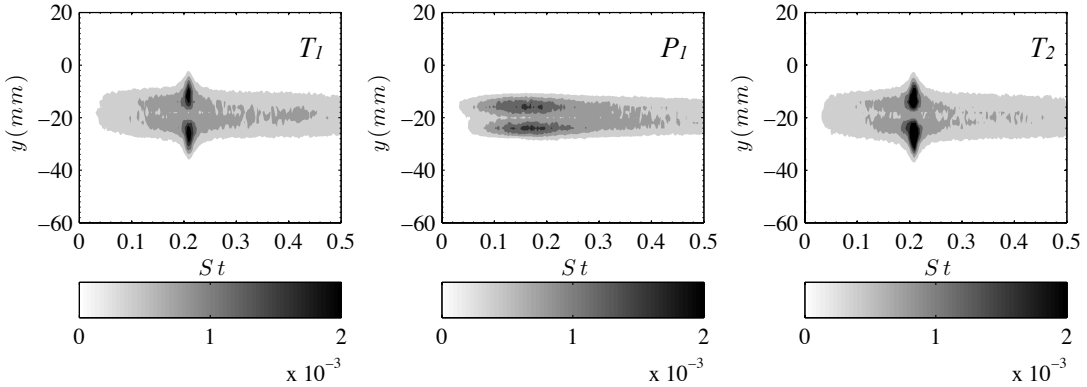

(a) Wing 3

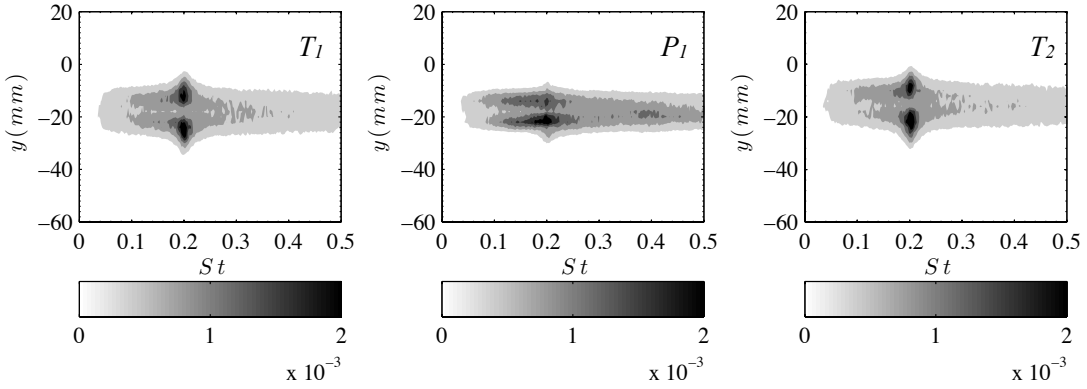

(b) Wing 6

Figure 4. Contour plot of pre-multiplied energy spectra (i.e. fE_{11}) at $x = 1.1c^*$ for successive *trough-peak-trough* locations (left to right) for Wings 3 and 6

to ε_{max}). Note that for Wing 1 we use the ε_{max} value for Wing 2 in order to obtain a non-zero value for the Strouhal number (since $\varepsilon_{max} = 0$ for Wing 1) and find that there is no appreciable peak in the energy spectra, as can be seen in figure 3(a). However a peak in the spectra, corresponding to the vortex shedding, is observed for all three span-wise positions in figure 3(b) for Wing 2, at a Strouhal number of $St_{vs} = f_{vs}\varepsilon_{max}/U_\infty = 0.189$, where f_{vs} is the frequency at which the vortex shedding occurs. This value is similar to the one obtained by Krentel & Nitsche,[5] but larger than the one obtained by Chong et al.[17] The first harmonic of the vortex shedding is also clearly visible as a second, dominant peak in figure 3, similar to what was observed previously.[5,17]

In figure 4, we plot the energy spectra for Wings 3 and 6 respectively. Again we note a clear peak that corresponds to the vortex shedding, however, the Strouhal number at which the vortex shedding is present (St_{vs}) appears to be higher than it was for Wing 2. The central figures correspond to data collected at a *peak* location on the trailing edges, where the thickness effectively comes down to a point and we would not expect to see a strong vortex shedding signature there, especially so close to the trailing

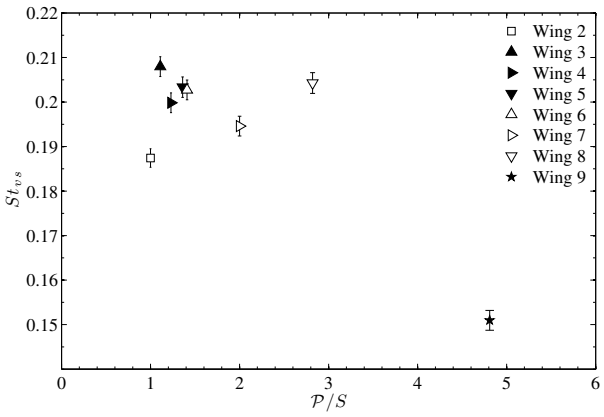

Figure 5. Vortex shedding Strouhal number ($St_{vs} = f_{vs}\varepsilon_{max}/U_\infty$) for Wings 2-9 obtained at $x = 1.1c^*$. Error bars denote resolution of measurements which are ± 0.002.

edge. The variation of vortex shedding Strouhal number, St_{vs}, for the different trailing edges is shown in figure 5. As mentioned earlier, we now see that the St_{vs} for Wings 3 and 6 are indeed higher than Wing 2, with the values being 0.208 and 0.203 for Wings 3 and 6 respectively compared to 0.189 for Wing 2. Note that the resolution of the measurements of the Strouhal number are ±0.002. As we decrease the chevron angle i.e. go from Wing 3 - 6 - 9, St_{vs} decreases. Chong et al[17] observed a similar trend with their trailing edges, however, we note a disparity between the data sets as we obtain $St_{vs} = 0.151$ for Wing 9, whereas Chong et al[17] find $St_{vs} \approx 0.13$ for the same trailing edge. Although we do observe an initial decrease in St_{vs} as the iteration is increased for both fractal dimensions, there is a noticeable increase for the last iteration. One obvious explanation for this increase is the larger ε_{max} that these two trailing edges (Wings 5 and 8) have (see table 1). Evidently, determining an appropriate physical length-scale to normalise the frequency data is not straight-forward. It is likely that this Strouhal number will change with the angle of attack α[22–24] and as shown by Chong et al,[17] Reynolds number. Note that the Reynolds number based on the maximum bluntness of the trailing edge is $Re_{\varepsilon_{max}} = U_\infty \varepsilon_{max}/\nu \approx 6,300$ and therefore of small enough value for a significant Reynolds number dependence of St_{vs} to exist. The vortex shedding would therefore have to be investigated at a number of angles of attack and Reynolds numbers in order to find the correct physical length-scale that would produce the same St_{vs} for all trailing edges.

B. Energy of vortex shedding

Having identified that there is a clear vortex shedding mechanism in the wake of all our wings except Wing 1, we now attempt to characterise the energy of the vortex shedding, following a similar method to Nedić

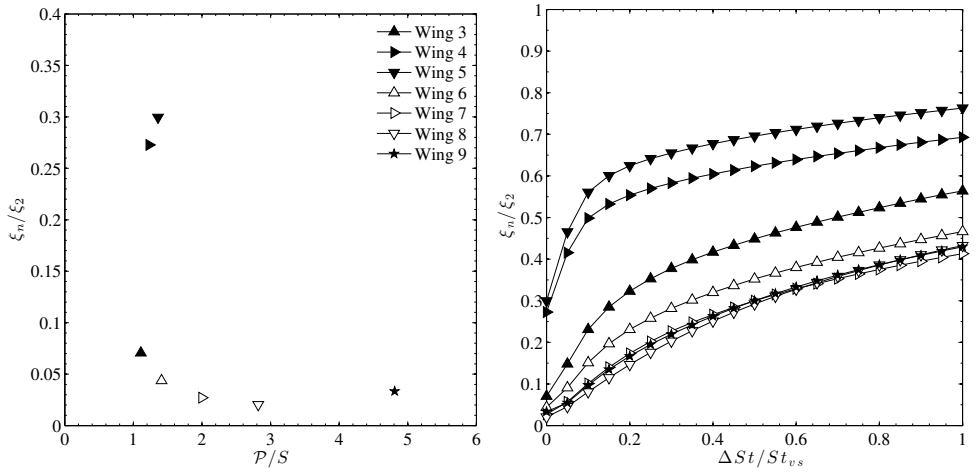

(a) At vortex shedding frequency (b) Range of frequency bandwidths

Figure 6. Vortex shedding energy of Wings 3-9 ($\xi_n, n = 3:9$) relative to Wing 2 (ξ_2) at (a) the vortex shedding frequency and (b) for a range of frequency bandwidths. Measurements taken at a downstream distance of $x = 1.1c^*$

et al.[20] The energy of the vortex shedding for a given downstream (x) and span-wise(z) location, E, is obtained by taking the energy spectra of the stream-wise fluctuating velocity component normalised with the free-stream velocity (E_{11}), and integrating the energy spectra about the vortex shedding Strouhal number over a given frequency bandwidth $\Delta St = St_2 - St_1$, where St_2 and St_1 are the upper and lower limits of the integration respectively such that $St_1 < St_{vs} < St_2$. By normalising the energy spectra with the free-stream velocity, we give an equal weighting to each y position and it also allows us to make a direct comparison between different wings at a given Reynolds number.

A value, $E_{vs}(x, y, z, \Delta St) = \int_{St_1}^{St_2} E_{11}(x, y, z, St)dSt$, can therefore be obtained for each wing-normal position (i.e. along y) and then integrated to obtain E for a given downstream (x) and span-wise location (z), as well as for a given frequency bandwidth (ΔSt) i.e.:

$$E(x, z, \Delta St) = \int_{-\infty}^{\infty} E_{vs}(x, y, z, \Delta St)dy \tag{8}$$

Since we only acquire measurements at three span wise locations and only observe a clear vortex shedding mechanism in the *trough* locations, we therefore only consider the average of the measurements taken at T_1 and T_2. Hence we define ξ, as shown in equation 9, as the average taken at two consecutive *trough* locations $z = T_k$ with $k = 2$ for our case.

$$\xi(x, \Delta St) = \frac{1}{k}\sum_{k=1}^{k} E(x, z = T_k, \Delta St) \tag{9}$$

In figure 6 we show the energy of the vortex shedding for all wings, normalised with the energy of the vortex shedding for Wing 2 (ξ_2). Two cases are shown; figure 6(a) shows the energy of the vortex shedding at the Strouhal number $St = St_{vs}$ i.e. $E(x, z, St_{vs}) = \frac{1}{k}\sum_{k=1}^{2}\int_{-\infty}^{\infty} E_{11}(x, y, z = T_k, St_{vs})dy$, and figure 6(b) shows the energy for a range of frequency bandwidths as defined in equation 9. Note that the values of ξ plotted in figure 6(a) correspond to $\Delta St/St_{vs} = 0$ in figure 6(b). We also limit our frequency bandwidth to $\Delta St = St_{vs}$ in figure 6(b) due to the harmonics that are present for Wing 2 (see figure 3), which is the wing we compare to.

First and foremost, all trailing edges show a significant reduction in the energy of the vortex shedding across all frequency bandwidths $\Delta St/St_{vs}$ compared to Wing 2, which has a uniform bluntness across the trailing edge. However, we also find a somewhat surprising result; as we increase the fractal iteration of the $D_f = 1.08$ family of trailing edges (Wings 3-5, denoted as solid triangles), the energy of the vortex shedding **increases**. As we increase the fractal dimension to $D_f = 1.33$ and hence make the base chevron sharper i.e. reduce the chevron angle, we find that these trailing edges (Wings 6-8, denoted as empty triangles) decrease the energy of the vortex shedding compared to Wing 3-5 (e.g. $D_f = 1.08$ and hence a broader base chevron angle), and that the energy of the vortex shedding **decreases** with increasing iteration for the $D_f = 1.33$ case. For example if we focus on the energy of the vortex shedding obtained using the largest frequency bandwidth ($\Delta St = St_{vs}$), then we find that the decrease in energy of the vortex shedding for Wing 6 compared to Wing 3 is roughly 18%, whilst the reduction between Wing 7 and Wing 6 is roughly 11%. At the vortex shedding frequency (figure 6(a)), these changes are considerably larger, with a 38% reduction between Wing 6 and Wing 3, and a further 38% reduction between Wing 7 and Wing 6. The same trend can be observed between our wings irrespective of the choice of frequency bandwidth used to determine the energy of the vortex shedding as shown in figure 6(b).

From Chong et al[17] we know that Wing 9 increases the sound pressure level (SPL) compared to a plain NACA0012 wing section (i.e. Wing 1) by as much as $\sim 10dB$ around the vortex shedding frequency, whilst across all other frequencies the reduction in SPL is $\sim 5.5dB$. Hence the noise generated by the vortex shedding is fairly significant. It may therefore be possible to gain some insights into how our wings may perform from an acoustic point of view by comparing the vortex shedding properties of our wings to those of Wing 9. In figure 6 we see that Wing 9 shows a significant reduction in the energy of the vortex shedding across all frequency bandwidths compared to Wing 2, however, only Wings 7 and

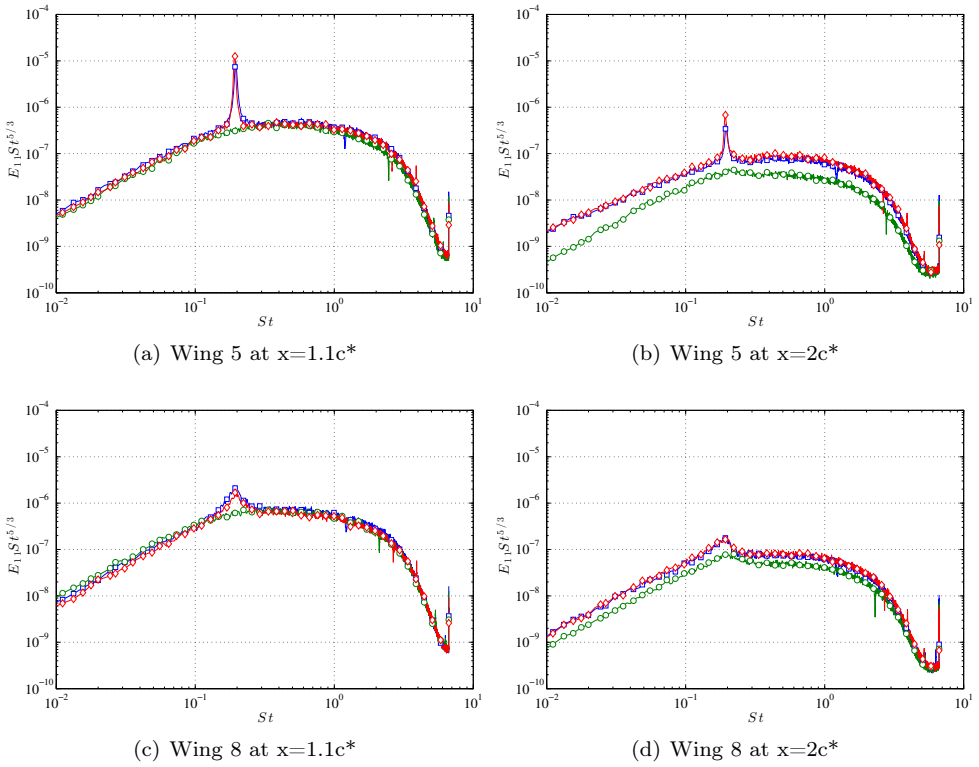

(a) Wing 5 at x=1.1c*

(b) Wing 5 at x=2c*

(c) Wing 8 at x=1.1c*

(d) Wing 8 at x=2c*

Figure 7. Energy spectra, compensated by $St^{5/3}$, for Wings 5 and 8, shown for the first and last downstream distance taken at $y = -10mm$. Symbols represent; Blue $\square - T_1$, Green $\bigcirc - P_1$, Red $\diamond - T_2$,

8 show a reduction in ξ compared to Wing 9. At the vortex shedding frequency, this can be as much as an 18% reduction for Wing 7 compared to Wing 9, and a 39% reduction for Wing 8 compared to Wing 9. Therefore it may be that these particular wings have reduced SPL around the vortex shedding frequency compared to Wing 9, but the acoustic tests of this must be left for a future study.

C. Downstream coherence of vortex shedding structures

One of the main reasons for having our hot-wires located at the $'trough - peak - trough'$ locations is to investigate whether there is any coherence in the vortex shedding across the span of the wing. For instance as we move downstream from our trailing edge, does the vortex shedding we observe in one trough interact with the vortex shedding in the other trough? To investigate this, the three hot-wires were moved to $y = -10mm$, since this gave a fairly strong signal in the energy spectra, and then traversed downstream from $x = 1.1c^*$ to $x = 2c^*$ in $0.1c^*$ intervals. In figure 7 we show the energy spectra at the first and last downstream locations for Wings 5 and 8, where we note, by compensating the spectra by $St^{5/3}$, that the wake is turbulent, or at least close to fully turbulent, in nature. For Wing 5, a clear spike is observed in the spectra for the hot-wires located in the *trough* locations (T_1 and T_2) at both

downstream positions, however, there is no clear sign that any vortex shedding is observed for the probe at the *peak* position (P_1). Similarly for Wing 8, vortex shedding is only found in the *troughs* at $x = 1.1c^*$ (figure 7(c)) whilst at $x = 2c^*$(figure 7(d)) there are signs that some vortex shedding is observed in the *peak* position, but it is not as energetic as the ones observed in the *troughs*. Note also that this figure clearly shows the reducing effect that increasing the fractal dimension D_f has on the energy of the vortex shedding. Figures 7(b) and 7(d) also show that the streamwise turbulent kinetic energy $\overline{u'^2}/U_\infty^2$ (which is the integral of the energy spectra) is higher in the *trough* locations compared to the *peak* locations, similar to what was observed by Krentel & Nitsche[5] for their blunt trailing edge modifications.

By examining the coherence coefficient $\gamma_{ij}(St)$, as defined in equation 10, we are able to ascertain how correlated the velocity signals are to each other. Note that in equation 10, C_{ij} is the cross power spectral density of the stream-wise velocity signals at span-wise positions i and j, whilst C_{ii} and C_{jj} are the energy spectra at positions i and j respectively. Since we are only interested in the vortex shedding, we investigate the coherence coefficient at this frequency, where $\gamma_{12}(St_{vs})$ is the correlation between the signals at T_1 and P_1 (at the vortex shedding Strouhal number), $\gamma_{23}(St_{vs})$ is the correlation between P_1 and T_2 and $\gamma_{13}(St_{vs})$ is the correlation between T_1 and T_2. The correlations for all downstream distances are shown in figure 8 for Wings 2, 3, 6 and 9, whilst in figure 9 we show them for Wings 2 and Wings 6, 7 and 8, the fractal wings with the greatest reduction in vortex shedding energy.

$$\gamma_{ij}^2(St) = \frac{|C_{ij}(St)|^2}{C_{ii}(St)C_{jj}(St)} \tag{10}$$

For all of our wings, except Wing 2, the coherence level between two successive troughs is negligible and can be deemed effectively zero within experimental uncertainty - figures 8(c) and 9(c). As a reminder, the position of the three hot-wire probes for Wing 9 are the same as for Wing 6-8, therefore the hot-wire probes are not located at successive $trough - peak - trough$ locations for this trailing edge. Although the centre probe is located at a peak location, the probes either side of it are at $z \approx \pm 2.35\lambda$, which would place them close to troughs. Nevertheless, even with such a large spacing of several wavelengths between two adjacent probes ($z \approx \pm 2.35\lambda$), the coherence level for Wing 9 increases with downstream distance, as shown in figures 8(a) and 8(b). Note that Chong et al,[17] who also examined the coherence at a downstream position of $x = 1.1c^*$, in fact plot γ_{12}^2 rather than γ_{12} and so a 'low' coherence level on their plot (figure 16b in[17]) is in fact a non-negligible coherence level. For example $\gamma_{12}^2 = 0.05$ gives $\gamma_{12} = 0.224$, which is similar to what we see at the same downstream position (although we are not able to verify

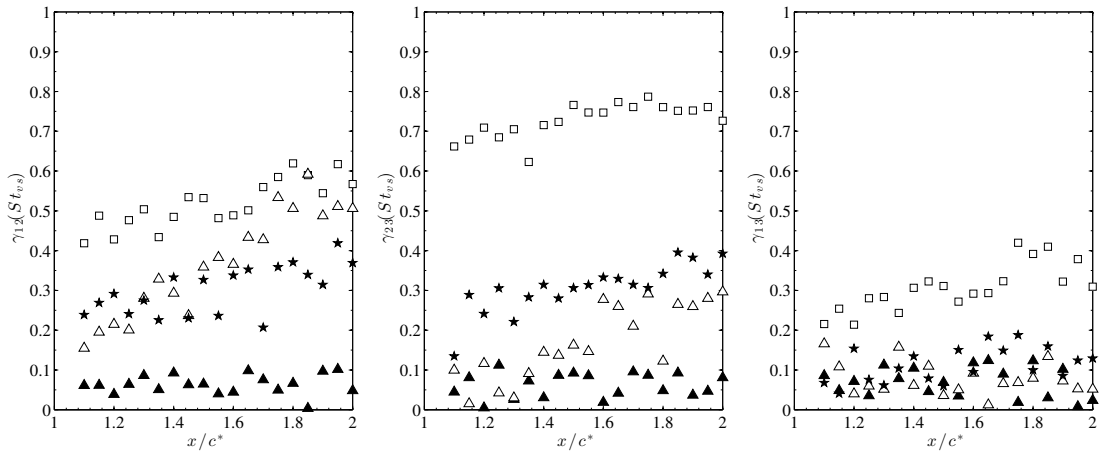

(a) $T_1 - P_1$ (b) $P_1 - T_2$ (c) $T_1 - T_2$

Figure 8. Coherence coefficient at vortex shedding frequency $\gamma_{12}(St_{vs})$ as a function of downstream distance for Wing 2(□), Wing 3(▲), Wing 6(△) and Wing 9(★) for two probes at (a) successive trough-peak location (b) peak and second trough location and (c) successive trough locations along the trailing edge of the wing.

if the y position is similar). The slow but steady increase in coherence levels as we move downstream suggests that the vortex shedding structure is becoming more correlated, but it does not appear that a single continuous structure exists along the span since the coherence level is effectively zero in figure 8(c).

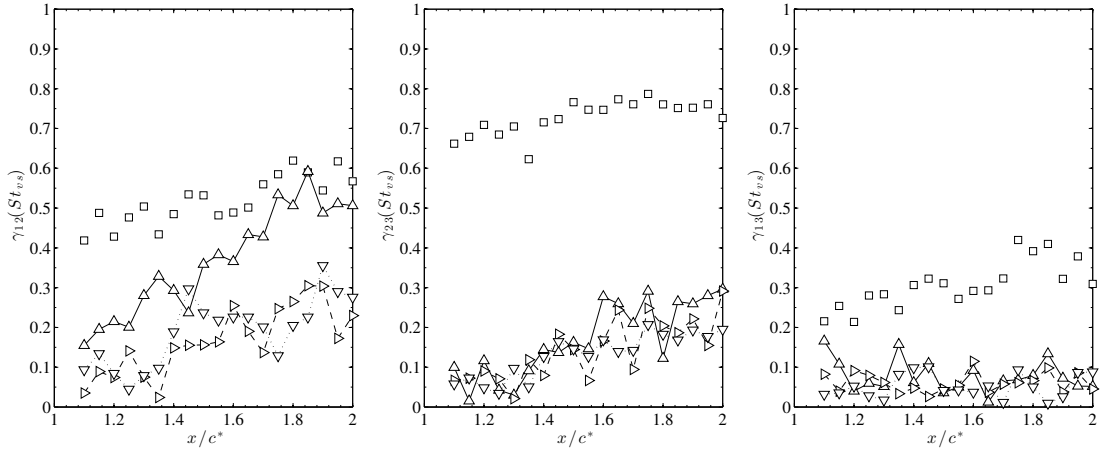

(a) $T_1 - P_1$ (b) $P_1 - T_2$ (c) $T_1 - T_2$

Figure 9. Coherence coefficient at vortex shedding frequency $\gamma_{12}(St_{vs})$ as a function of downstream distance for two probes at (a) successive trough-peak location (b) peak and second trough location and (c) successive trough locations along the trailing edge of the wing. Data shown for D_f = 1.33 family of trailing edges i.e. Wings 6-8 (△, ▷, ▽ respectively) as well as Wing 2(□) for comparison.

Figure 8 clearly shows that the coherence levels for Wing 3 are effectively zero for all downstream positions and probe configurations, the same is true for the next two iterations of that particular fractal/multi-scale pattern (Wings 4 and 5). Owing to the manner in which the coherence measurements were taken, that lack of any strong coherence in figure 8 for these wings would imply that the vortex

shedding structures, which are clearly present and have more energy than Wings 6-9 for example (see figure 6), are more three-dimensional in nature. If we increase the fractal dimension to D_f = 1.33 (Wing 6-8), we note that the coherence levels start to build up as we move downstream when considering two adjacent probes. This would imply that the vortex shedding structure is detected in the peak regions, exactly as was shown in figure 7, however, as the fractal iteration increases, the coherence levels drop suggesting that these particular trailing edges are breaking down, or even possibly delaying, the interaction of vortex structures from successive trough locations. This is again in-line with what was observed in figure 6 where the energy of the vortex shedding decreases with increasing iteration.

IV. Aerodynamic performance

It is known that by truncating the wing section i.e. removing part of the trailing edge, the maximum lift coefficient $C_{L_{max}}$ increases.[2,3,5] On the other hand, by adding a undulating leading edge it has been shown by Rostamzadeh et al[12] , for example, that there is a reduction in the maximum lift coefficient compared to the base-line case, however the stall angle is increased. Chong et al[17] demonstrated that it is possible to alter the acoustic signature of the wing with trailing edge modifications similar to Wings 3, 6 and 9, however, from an engineering point of view, it is important to also characterise the aerodynamic performance.

In figure 10, we show the variation of the lift coefficient, $C_L = L/(q_\infty Sc)$ where $q_\infty = \frac{1}{2}\rho U_\infty^2$, with angle of attack for all trailing edges, as well as the drag coefficient, $C_D = D/(q_\infty Sc)$. As a reminder, c is the mean chord of the wing, as defined in equation 5, hence Sc is the area of the airfoil. Immediately we note two key results: by truncating the trailing edge of the NACA0012 wing section to create a blunt trailing edge, we increase $C_{L_{max}}$, in agreement with previous measurements.[2,3,5] Secondly, all the serrated edges have a lower $C_{L_{max}}$ compared to the blunt trailing edge (Wing 2), but a higher $C_{L_{max}}$ than the plain NACA0012 trailing edge (Wing 1). Although it is difficult to determine whether or not there is any measurable change in the drag coefficient for the serrated trailing edges, it is clear that the blunt trailing edge (Wing 2) has a larger drag coefficient compared to the other trailing edges.

The change in lift coefficient compared to the base NACA 0012 wing section (Wing 1) is shown in figure 11, with figure 11(a) showing the change for the D_f = 1.08 trailing edges, figure 11(b) for the D_f = 1.33 trailing edges and figure 11(c) for the chevron based trailing edges (Wings 3, 6 and 9). Note that the error bars in the figures are the standard deviations from the ten runs and that the dashed lines

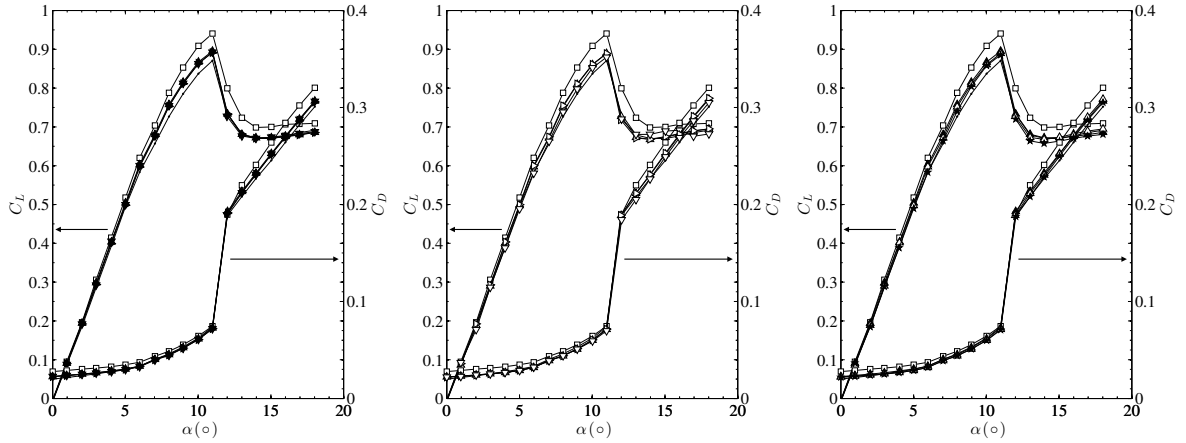

(a) Wings 3(▲), 4(▶) and 5(▼) (b) Wings 6(△), 7(▷) and 8(▽) (c) Wings 3(▲), 6(△) and 9(★)

Figure 10. Variation of lift and drag coefficient with angle of attack for (a) D_f = 1.08 family of trailing edges (b) D_f = 1.33 family of trailing edges and (c) chevron trailing edges. Note that Wing 1(•) and Wing 2(□) are present in all three sub-plots for reference

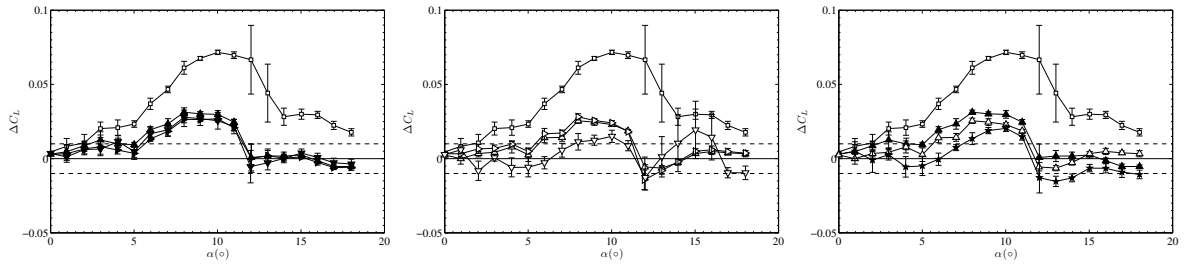

(a) Wings 3(▲), 4(▶) and 5(▼) (b) Wings 6(△), 7(▷) and 8(▽) (c) Wings 3(▲), 6(△) and 9(★)

Figure 11. Change in lift coefficient compared to Wing 1 for (a) D_f = 1.08 family of trailing edges (b) D_f = 1.33 family of trailing edges and (c) chevron trailing edges. Wing 2(□) shown as a reference case in all figures. Dashed lines indicated maximum measurement uncertainty

are the maximum measurement uncertainty. Here, the change in C_L is clearer to see and we note what appears to be a clear dependence on chevron angle, with the lift coefficient increasing as the chevron angle φ increases, particularly as the wing approaches stall and the data lie outside the measurement uncertainty - figure 11(c). Hence this suggests that to maximise lift, it is preferable to have a 'smoother' trailing edge serration i.e. Wing 3 which has a lower fractal dimension of D_f = 1.08 compared to Wing 6 which has a fractal dimension of D_f = 1.33. In figure 11(a) we show the change in lift coefficient for the D_f = 1.08 family of trailing edges. Although the data for the three fractal iterations are buried within the error bars, the trend that emerges is one similar to that seen in figure 11(c) - by increasing the perimeter, and hence increasing the fractal iteration in this instance, we are decreasing the lift. A similar trend is observed for the D_f = 1.33 family of trailing edges in figure 11(b), although it appears

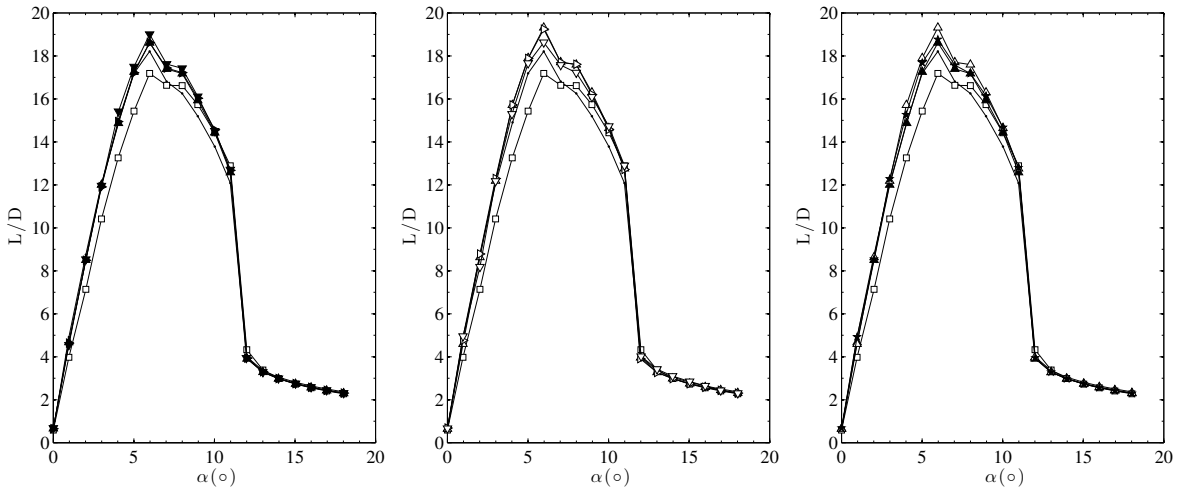

(a) Wings 3(▲), 4(▶) and 5(▼) (b) Wings 6(△), 7(▷) and 8(▽) (c) Wings 3(▲), 6(△) and 9(★)

Figure 12. Variation of lift-to-drag ratio with angle of attack for (a) D_f = 1.08 family of trailing edges (b) D_f = 1.33 family of trailing edges and (c) chevron trailing edges. Note that Wing 1(•) and Wing 2(□) are present in all three sub-plots for reference

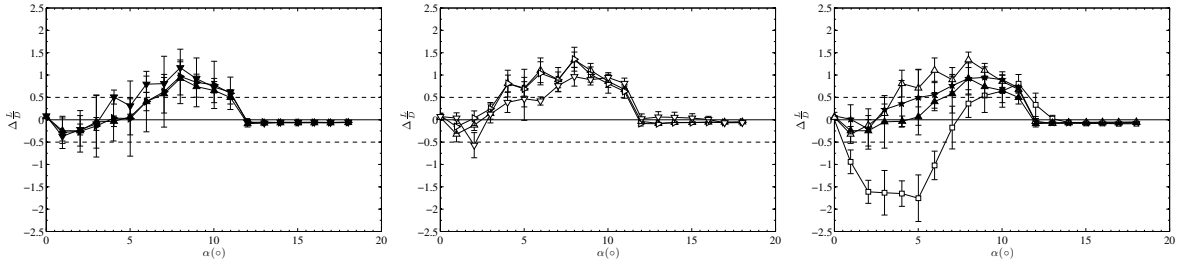

(a) Wings 3(▲), 4(▶) and 5(▼) (b) Wings 6(△), 7(▷) and 8(▽) (c) Wing 2(□), Wings 3(▲), 6(△) and 9(★)

Figure 13. Change in lift-to-drag ratio compared to Wing 1 for (a) D_f = 1.08 family of trailing edges (b) D_f = 1.33 family of trailing edges and (c) chevron trailing edges and Wing 2. Dashed lines indicated maximum measurement uncertainty.

that Wing 7 shows a marginal increase in C_L compared to Wing 6 for small angles of attack.

To accurately quantify the change in aerodynamic performance of these wings, we plot the lift-to-drag ratio (L/D) and the change in lift-to-drag ratio (L/D) compared to Wing 1 in figures 12 and 13 respectively. Although the blunt trailing edge (Wing 2) produces a higher C_L compared to the NACA 0012 wing, the associated increase in drag coefficient results in an overall drop in aerodynamic performance at lower angles of attack i.e. the lift-to-drag ratio decreases - see figure 13(c). Immediately prior to stall we note that Wing 2 shows a slight improvement in the lift-to-drag ratio. If we compare the chevron based trailing edges in figure 13(c), we find that Wing 6 has the highest L/D ratio, suggesting that its drag coefficient must be smaller than the D_f = 1.08(1). This would collaborate with figure 6(a) where the vortex shedding energy is lower for Wing 6 compared to Wing 3, hence one would expect the drag coefficient to be smaller.[4–6] In figure 13(a) we show the change in performance for Wings

3-5, where we note that the aerodynamic performance reduces with increasing perimeter and therefore fractal iteration, except with Wing 5 showing a slight improvement in L/D at low angles of attack. All three iterations of the D_f = 1.33 trailing edges (Wings 6-8) are shown in figure 13(b), where a similar trend is observed and where the results around the stall angle all lie outside our estimated measurement uncertainty.

With the results presented here, two conclusions can be made: an optimal change in aerodynamic performance can be achieved by using a chevron based trailing edge alone, however, this change in performance appears to be sensitive to the angle (φ) used for the chevron pattern. We also conclude that Wing 9 (Wing S2 in[17]) shows a slight improvement in the aerodynamic performance, and based on the findings of Chong et al,[17] also a reduction in the high frequency noise. Finally, by adding fractal iterations to a chevron pattern, we find that they do not improve, nor significantly diminish, the improvement in aerodynamic performance that the chevron creates in the first place. However, they do decrease the vortex shedding intensity.

V. Discussion and Conclusion

From the outset, the main aim of this study was to investigate the feasibility of using fractal/multi-scale trailing edges to modify the vortex shedding structures generated by the wing. Although we focused on the vortex-shedding in the *trough* areas, it is clear that increasing the fractal iteration decreases the energy of the vortex shedding, but only if the fractal dimension D_f is large enough i.e. chevron angle φ is small enough. For $\varphi > 45°$, adding a fractal/multi-scale pattern to the trailing edge increases the energy of the vortex shedding, whilst for $\varphi \leq 45°$, the energy of the vortex shedding decreases.

From the coherence measurements it would appear that there is virtually no correlation in the signal between successive $trough - peak - trough$ locations for Wings 3-5 (D_f = 1.08, φ = 64.54°), suggesting that the vortex shedding is more three-dimensional in nature as opposed to the clear longitudinal vortex shedding observed for Wing 2 for example. It is believed that the initial reduction in ξ that we see in figure 6(a) may be due to the amount of bluntness that is exposed to the flow. For example, Wing 2 has a uniform bluntness of $\varepsilon = 5.56mm$ along the span, but for Wing 3, this bluntness only exists at a single span-wise location within a given wavelength i.e. $z = 0.25\lambda$. As we start adding iterations to the pattern, this maximum bluntness (for 2h=20mm) appears more often as can be seen in figure 2 and it is conceivable that there would be an increase in the strength of the vortex shedding due to this.

Although a similar argument could be given for Wings 6-8 (D_f = 1.33, φ = 45°), it is possible that the proximity of all the length-scales to each other would make the trailing edge act as a more efficient mixing/vortex breakdown mechanism than for Wings 3-5 where they are further away from each other i.e. the $\lambda/2h$ value is smaller for Wings 6-8. This argument is strengthened by the coherence measurements in figure 9 where the coherence levels are comparatively large, but decrease with increasing fractal iteration. It should also be re-iterated that Wings 7 and 8 had a larger reduction in ξ compared to Wing 9, which is known to reduce high frequency noise. At the vortex shedding frequency, this can be as much as an 18% reduction for Wing 7 compared to Wing 9, and a 39% for Wing 8 compared to Wing 9.

Finally, we were able to complement the study by Chong et al[17] and show that Wing 9 (S2 in[17]) increases the lift-to-drag ratio for a large range of angles of attack. The lift-to-drag ratio can be improved by increasing the chevron angle and the addition of a fractal/multi-scale trailing edge does not significantly improve nor hamper the improved aerodynamic performance of the chevron based design.

From our measurements, Wings 7 and 8 produced the best combination in performance, by reducing the energy of vortex shedding and increasing the maximum lift-to-drag ratio (compared to Wing 1) by 8% and 6.7% respectively. In order to fully understand the acoustic properties of such trailing edges, one would obviously need to take acoustic measurements as well as more complex coherence measurements in the wake to fully understand the vortex shedding structures and the manner in which they are shed. If, however, we assume for the time being that a reduction in the intensity of the vortex shedding causes a reduction in the low-frequency noise it generates, as suggested by Chong et al,[17] our measurements therefore suggest that using fractal/multi-scale trailing edges may prove to be beneficial for both aerodynamic and acoustic performance. Fractal wings also have a potential to act as quiet air brakes and spoilers, perhaps even more promising than the fractal porosity spoilers recently proposed by Nedić et al.[25]

Acknowledgements

The authors were supported by an ERC Advanced Grant (2013-2018) awarded to J.C. Vassilicos

References

[1]Smith, H. A. and Schaefer, R. F., "Aerodynamic Characteristics at Reynolds Numbers of 3.0 x 10 (6) and 6.0 x 10 (6) of Three Airfoil Sections Formed by Cutting Off Various Amounts From the Rear Portion of the NACA 0012 Airfoil

Section," Tech. rep., NACA TN-2074, 1950.

[2]Standish, K. J. and Van Dam, C. P., "Aerodynamic analysis of blunt trailing edge airfoils," Journal of solar energy engineering, Vol. 125, 2003, pp. 479.

[3]Tanner, M., "A method for reducing the base drag of wings with blunt trailing edge," Aeronaut Quart, Vol. 23, 1972, pp. 15–23.

[4]Rodriguez, O., "Base drag reduction by control of the three-dimensional unsteady vortical structures," Experiments in Fluids, Vol. 11, No. 4, 1991, pp. 218–226.

[5]Krentel, D. and Nitsche, W., "Investigation of the near and far wake of a bluff airfoil model with trailing edge modifications using time-resolved particle image velocimetry," Experiments in Fluids, Vol. 54, No. 7, 7 2013.

[6]Tombazis, N. and Bearman, P. W., "A study of three-dimensional aspects of vortex shedding from a bluff body with a mild geometric disturbance," Journal of Fluid Mechanics, Vol. 330, 1997, pp. 85–112.

[7]Werle, M. J., Paterson, R. W., and Presz Jr, W. M., "Trailing-edge separation/stall alleviation," AIAA journal, Vol. 25, No. 4, 1987, pp. 624–626.

[8]Miklosovic, D. S., Murray, M. M., Howle, L. E., and Fish, F. E., "Leading-edge tubercles delay stall on humpback whale (Megaptera novaeangliae) flippers," Phys. Fluids, Vol. 16, No. 5, 2004, pp. L39.

[9]Johari, H., Henoch, C. W., Custodio, D., and Levshin, A., "Effects of Leading-Edge Protuberances on Airfoil Performance," AIAA Journal, Vol. 45, No. 11, 11 2007, pp. 2634–2642.

[10]van Nierop, E., Alben, S., and Brenner, M., "How Bumps on Whale Flippers Delay Stall: An Aerodynamic Model," Physical Review Letters, Vol. 100, No. 5, 2 2008.

[11]Hansen, K. L., Kelso, R. M., and Dally, B. B., "Performance Variations of Leading-Edge Tubercles for Distinct Airfoil Profiles," AIAA Journal, Vol. 49, No. 1, 1 2011, pp. 185–194.

[12]Rostamzadeh, N., Kelso, R. M., Dally, B. B., and Hansen, K. L., "The effect of undulating leading-edge modifications on NACA 0021 airfoil characteristics," Physics of Fluids, Vol. 25, No. 11, 2013, pp. 117101.

[13]Howe, M. S., "Aerodynamic noise of a serrated trailing edge," Journal of Fluids and Structures, Vol. 5, No. 1, 1991, pp. 33–45.

[14]Oerlemans, S., Fisher, M., Maeder, T., and Kögler, K., "Reduction of Wind Turbine Noise Using Optimized Airfoils and Trailing-Edge Serrations," AIAA Journal, Vol. 47, No. 6, 6 2009, pp. 1470–1481.

[15]Gruber, M., Joseph, P. F., and Chong, T. P., "On the mechanism of serrated airfoil trailing edge noise reduction," AIAA Paper 2011-2781, 2011.

[16]Jones, L. E. and Sandberg, R. D., "Acoustic and hydrodynamic analysis of the flow around an aerofoil with trailing-edge serrations," Journal of Fluid Mechanics, Vol. 706, 9 2012, pp. 295–322.

[17]Chong, T. P., Vathylakis, A., Joseph, P. F., and Gruber, M., "Self-Noise Produced by an Airfoil with Nonflat Plate Trailing-Edge Serrations," AIAA Journal, Vol. 51, No. 11, 11 2013, pp. 2665–2677.

[18]Geyer, T., Sarradj, E., and Fritzsche, C., "Measurement of the noise generation at the trailing edge of porous airfoils," Experiments in Fluids, Vol. 48, No. 2, 2 2010, pp. 291–308.

[19]Nedić, J., Ganapathisubramani, B., and Vassilicos, J. C., "Drag and wake characteristics of flat plates perpendicular to the flow with fractal edge geometries," Fluid Dynamics Research, Vol. 45, No. 6, 12 2013, pp. 061406.

[20]Nedić, J., Supponen, O., Ganapathisubramani, B., and Vassilicos, J., "Geometrical influence on vortex shedding in turbulent axisymmetric wakes," Physics of Fluids (1994-present), Vol. 27, No. 3, 2015, pp. 035103.

[21]Nedić, J., Vassilicos, J. C., and Ganapathisubramani, B., "Axisymmetric turbulent wakes with new non-equilibrium similairty scalings," Phys. Rev. Lett., Vol. 111, No. 14, 10 2013, pp. 144503.

[22]Chen, J. M. and Fang, Y. C., "Strouhal numbers of inclined flat plates," Journal of wind engineering and industrial aerodynamics, Vol. 61, No. 2, 1996, pp. 99–112.

[23]Huang, R. F. and Lin, C. L., "Vortex shedding and shear-layer instability of wing at low-Reynolds numbers," AIAA journal, Vol. 33, No. 8, 1995, pp. 1398–1403.

[24]Yarusevych, S. and H. Boutilier, M. S., "Vortex Shedding of an Airfoil at Low Reynolds Numbers," AIAA Journal, Vol. 49, No. 10, 10 2011, pp. 2221–2227.

[25]Nedić, J., Ganapathisubramani, B., Vassilicos, J. C., Boree, J., Brizzi, L.-E. . E., and Spohn, A., "Aeroacoustic performance of fractal spoilers," AIAA journal, Vol. 50, No. 12, 2012, pp. 2695–2710.